Optimal Control of Automatic Transmission based on Optimization of Constant Accelerator Maneuvers

A. Alizadegan, K. Barton, D. Tilbury

Mechanical Engineering Department, University of Michigan, Ann Arbor, Michigan 48109

Abstract— **This paper aims at designing a feedback optimal gear-shift control for discrete-ratio powertrains equipped with automatic transmission (AT) and electronic throttle control (ETC). The objective is to maximize fuel efficiency while considering driveability concerns. The accelerator is interpreted as desired wheel power. The gear-shift control is coordinated with ETC to satisfy the power demand. Feedback tables are designed based on optimization of the constant accelerator maneuver with Dynamic Programming (DP) algorithm. A technique is proposed to include the torque-converter loss in the single-state dynamic model of the vehicle in constant accelerator maneuvers. Real-time performance of the gear-shift control is evaluated by contrasting the simulation results with solution of the optimization problem for some arbitrary maneuvers. Fuel economy and driveability of the proposed controller are quantitatively analyzed by quasi-static simulation for some benchmark driving cycles.**

Index Terms— **Automatic transmission (AT), gear-shift map, dynamic programming (DP), drivability, fuel economy, electronic throttle control (ETC), Integrated powertrain control**

1 INTRODUCTION

In the last few decades, innovations in gear-shift controller design for automatic transmissions (AT) has been on "hot" spot of automotive industry to address driver comfort [1] from one side and fuel economy and emission requirements from the other [2]. Compared to continuously variable transmissions (CVT), gear-shift control in descrete-ratio transmissions plays an even more vital role in vehicle performance because operating point of the powertrain changes greatly in a step way depending on the gear-shift decision. Hence, gear-shift strategy plays an important role in performance of the vehicle.

Fuel economy and driveability are the most important performance indexes of the powertrain. Requirements for these performance indexes commonly contradict. Fuel economy requires gear-shifts to take place in low vehicle speed because engine and torque-converter loss is lower in low engine RPM; however, lower engine RPM does not provide enough power to satisfy driveability requirements. So usually some fuel economy is sacrificed to meet certain driveability standards. For a CVT-based powertrain, Serrarens [3] suggests that 15-20% increase in fuel economy compared to engine's maximum fuel efficiency curve leads to an acceptable driveability.

To consider driveability in a more quantitative way, different definitions of driveability has been proposed. Traditionally, some researches correlated driveability with desired drive torque [4-7]; however, a research by Vahabzadeh and Linzell [8] correlates the driver's accelerator input with desired engine power, putting focus of driveability issues on power availability and delivery. Power availability

interpretation concerns vehicle's acceleration potential. To consider power availabity, Ngo *et al.* [9] define driveability as power reserve which is the difference between engine's current power and maximum achievable power. Power delivery concerns driver's power demand satisfaction. This interpretation is considered by Kim *et al.* [10] by defining the driveability as engine power. With respect to a consistent and desirable vehicle response under different driving conditions, Smith *et al.* [11] defines the driveability as change in engine power reserve for a given change in the throttle angle. For powertrains featured with torque-converter, the drawback of driveability definitions based on engine power is that they cannot capture the torque-converter loss.

It is established that integrated control transmission and engine can address stricter fuel economy and driveability requirements [12]. Specifically, since accelerator is no longer mechanically linked to the throttle, it is interpreted as driver's demand and throttle is controlled to achieve that objective. As more and more vehicles are getting equipped with electronic throttle control (ETC), this approach is getting more attention in the literature. For instance, Sakaguchi *et al.* [13] developes an algorithm for vehicles equipped with ETC and CVT that calculates the engine torque and CVT ratio combinations achieving the highest overall efficiency. The drawback of these representations is that they cannot consider the torque-converter loss affecting output of the engine.

Owing to the discrete nature of the gear-shift, discrete-time optimization technique, e.g. dynamic programming (DP) [14], [15], [16], [17], are widely adopted in the gear-shift control problem [9, 10, 18-22]. The most prominent advantage of DP algorithm related to the integrated control approach and driveability considerations is its capability to accommodate equality/inequality constraints and multi-objective optimization. For example, Ngo *et al.* [9] includes power reserve in the DP algorithm using two methods. In the first method, weighted inverse of the power reserve is summed with weighted fuel consumption in the objective function. In the second method, an inequality constraint is imposed as minimum allowable power reserve. Kim *et al.* [10] imposes equality constraints on engine power while optimizing for fuel economy on constant accelerator maneuvers to satisfy driver's power demand set by accelerator in an ETC-based powertrain. On the flipside, DP algorithm suffers from two major disadvantages. First, it can derive optimal gear-shift schedule for a priori given driving cycle only. The gear-shift schedule derived with this technique does not have a feedback structure. Therefore, it is not real-time implementable. Real-time implementable control of gear-shift has revolved around gear-shift maps designed based on empirical experiments [23],

heuristic suboptimal rule-based methods such as genetic algorithm, fuzzy logic [24, 25], learning algorithms, or pattern recognition [26]. Globally optimal gear-shift strategies based on DP are only used to benchmark fuel economy on certain driving cycles. Another drawback of the DP algorithm is its high computational cost. Based on these, it is efficient for models with low number of state variables and control inputs such as quasi-static models [19] to be used as benchmark for fuel economy. The downside with quasi-static model is that it ignores fast dynamics in powertrain such as torque-converter (or clutch) slipping which has significant impact on fuel economy.

Aiming at a real-time implementable fuel-optimal controller, this work proposes design of integrated gear-shift/throttle maps based on optimization of constant accelerator maneuvers for fuel economy. Accelerator input is interpreted as driver's wheel power demand to account for the torque-converter loss. This input is considered in the objective function of the optimization problem to represent driver's power demand satisfaction in the controller design stage. Furthermore, based on this interpretation, the time scale separation between torque converter dynamics and vehicle dynamics are exploited to develop a single-state model alleviating the computational load of the DP algorithm. To account for the torque converter loss during gear-shift, a novel representation of torque-converter loss in the cost function is proposed. The optimization results for different accelerator levels are then combined in a gear-shift map form for real-time implementation.

In the next section, dynamic model of the vehicle is described. Section 3 proposes an analytical analysis of a constant accelerator maneuver based on the wheel power interpretation of the accelerator. Section 4 presents a formal statement of the optimization problem which is the basis of the feedback table design. The solution of the optimization problems are used in section 5 to design the integrated gear-shift and throttle feedback table. In section 6 optimality of the gear shift feedback table is evaluated by contrasting the simulation and optimization results of the DP algorithm for some benchmark maneuvers. Furthermore, through quasi-static simulations, gear-shift control of the proposed controller is compared with the standard gear-shift pattern. The effect of gear-shift hysteresis on the fuel efficiency and driveability of the control strategy are studied in the quasi-static simulations.

2 VEHICLE DYNAMIC MODEL

This section describes the vehicle's dynamic model. This model is based on the model developed in [10] for a two-wheel drive production pickup truck with a 5.3-L V8 engine equipped with ETC and four-speed AT. This model is relatively detailed, so it is not used for optimizations; however, it will be used as plant for simulations because its adequate correspondence to the target vehicle has been verified in [10] through wide open throttle (WOT) and environmental protection agency (EPA) tests. As shown in Fig. 1. The model encompasses four subsystems, namely, engine, torque converter, gearbox, and body.
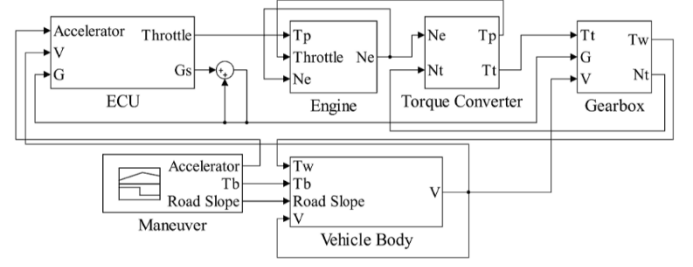

Fig. 1. Vehicle dynamic model

2.1 ECU

Fig. 2 shows the configuration of ECU used in this work. As shown, ECU uses accelerator (ξ), gear (G) and velocity (V) feedbacks to control the gear-shift (G_s) and throttle.
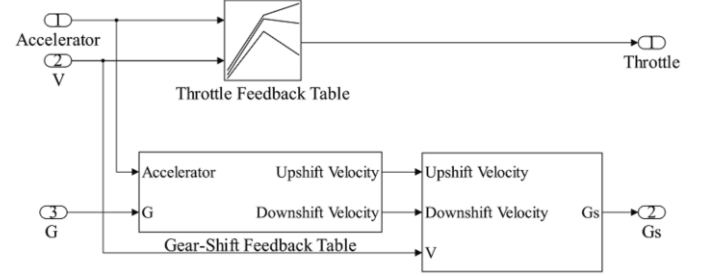

Fig. 2. ECU Configuration

For a certain accelerator, the gear-shift feedback table specifies the optimal up-shift and down-shift velocities for the currently engaged gear. The gear-shift decision is made by comparison of the velocity feedback with the optimal up-shift and down-shift velocities. Throttle (δ) is controlled based on the accelerator and velocity feedback. Detailed design of the gear-shift and throttle feedback tables is addressed in this work.

2.2 Engine

The governing differential equation of engine RPM (N_e) is:

$$\dot{N}_e = \frac{60}{2\pi} \frac{(T_e - T_p)}{(J_e + J_p)} \tag{1}$$

In the equation above, T_e, J_e are, respectively, torque and rotational moment of inertia of the engine. T_p and J_p are respectively, torque and rotational moment of inertia of the torque-converter pump. The engine torque is obtained from the engine torque diagram as a function of throttle and engine RPM. Fig. 3 (a) shows the engine torque diagram. As shown, the engine torque increases with the throttle and decreases with the engine RPM.

Fig. 3 (b) shows the fuel consumption diagram of the engine. In this diagram, $\dot{m}$ is the fuel consumption rate which is a function of the throttle and the engine RPM. As shown, the fuel consumption rate increases both with throttle and engine RPM.

Fig. 3 (c) shows the engine power diagram. For a certain throttle, the engine power has a maximum point as a function of the engine RPM. At low engine RPM, the engine loss is due to the combustion inefficiency. At high engine RPM, the engine loss is due to the friction of mechanical elements in the

engine. The engine diagrams are based on the engine tests given in [10].
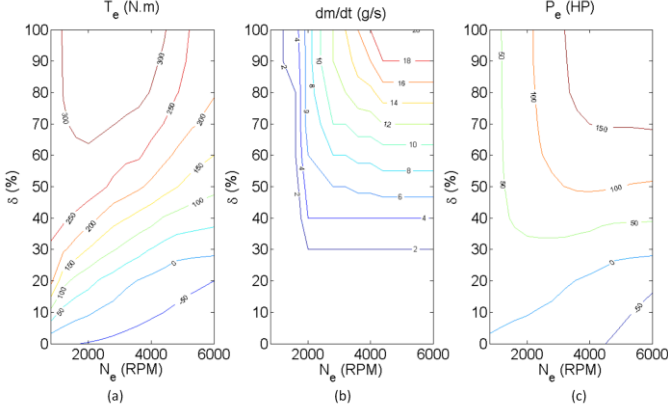

Fig. 3. Engine Characteristic Diagrams [10] (a) Engine Torque Diagram (b) Engine Fuel Consumption Diagram (c) Engine Power Diagram

Based on [10] the operation limit of the engine is 600 to 6000 RPM.

2.3 Torque Converter

The torque converter encompasses a pump which is connected to the engine output shaft, a turbine connected to the gearbox input shaft, and a stator grounded to a one-way clutch. The torque converter is represented by a static nonlinear input-output model as (2) and (3).

$$T_p = (N_e/K)^2 \tag{2}$$
$$T_t = r_T T_p \tag{3}$$

In these equations, T_p and T_t are respectively the pump and turbine torques. K is the torque converter capacity factor, and r_T is the torque ratio of the torque converter. K and r_T are functions of slipping ratio (r_s). The slipping ratio is defined as the speed ratio between the input and output shafts of the torque converter:

$$r_s = N_t/N_e \tag{4}$$

In the present work, the experimental torque converter characteristic diagrams from [10] are modeled as analytical equations to be used in analysis. The torque converter characteristic parameters are modeled as:

$$K = a + b/(r_s - 1) \tag{5}$$
$$r_T = c + dr_s \tag{6}$$

Torque converter has different behavior for $0 < r_s < 1$ and $r_s > 1$.

TABLE I. TORQUE CONVERTER CHARACTERISTIC PARAMETERS

Parameter	$0 < r_s < 1$	$r_s > 1$
a	92.2	103.6
b	-3.5	12.4
c	1.9	1
d	-0.9	0

As such, the parameters a, b, c, and d take different values depending on the range of the slipping ratio. Table I shows the entries used for the parameters of the proposed model.

Fig. 4 shows the experimental torque converter characteristic diagrams compared to their model.
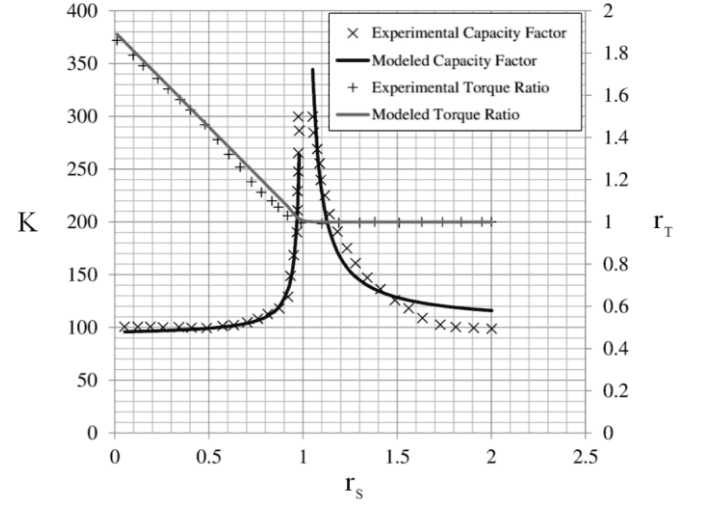

Fig. 4. Torque-converter characteristic model compared to the experimental data [10]

The torque converter loss occurs due to the viscosity of the rotating fluid.

2.4 Gearbox

As such, the state equation for gear is, a discrete-time equation as:

$$G^+ = G^- + G_s \tag{7}$$

Gearbox is simply modeled by a linear input-output system. The final gear ratio (r_f) is the multiplication of final drive ratio (r_{fd}) and gear ratio (r_G).

$$r_f = r_G r_{fd} \tag{8}$$

Gear ratio is a function of the gear. Final drive ratio is a constant parameter. The values for gear ratio of each gear and the final drive ratio are shown in Table III. The gear efficiency (η_G) and final drive efficiency (η_{fd}) represent the torque transmission efficiency of the gearbox. The final torque transmission efficiency (η_f) can be calculated as:

$$\eta_f = \eta_G \eta_{fd} \tag{9}$$

The wheel torque (T_w) and turbine RPM (N_t) can be calculated by using (10) and (11). The wheel RPM (N_w) is obtained from the longitudinal dynamics of the vehicle body discussed in the next section.

$$T_w = \eta_f r_f T_t \tag{10}$$
$$N_t = r_f N_w \tag{11}$$

It is not possible to calculate the turbine RPM directly from the torque converter dynamics because the rotational moment of inertia of the turbine shaft is neglected. Therefore, it is obtained in a reverse calculation manner using (11).

2.5 Vehicle Body

For vehicle body only the longitudinal dynamics is considered because it governs the fuel economy of the vehicle. Fig. 5 represents the free body diagram of the vehicle body. The inertial forces/moments are assigned according to the D'Alemberts's principle. These forces are designated with dashed arrows.
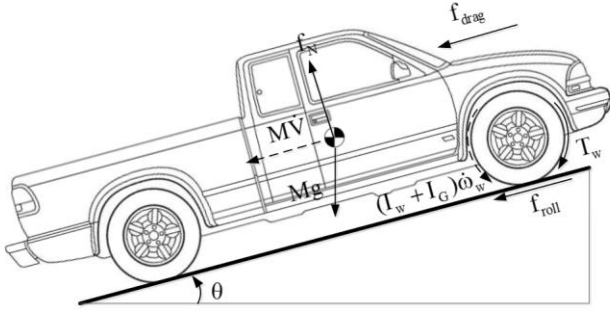
Fig. 5. Vehicle body free body diagram

In Fig. 5, aerodynamic drag (f_{aero}), rolling friction (f_{roll}), are modeled as:

$$f_{drag} = 0.5\rho C_D A V^2 \tag{12}$$

$$f_{roll} = K_r f_N \tag{13}$$

In (12) A is the frontal area, C_D is the drag coefficient, and ρ is the air density. In (13) K_r is the rolling friction coefficient, and f_N is the normal surface reaction. T_w is the total wheel torque. $M\dot{V}$ and $(I_w + I_G)\dot{\omega}_w$, respectively, represent the body and powertrain inertia. M is the vehicle mass. I_w is the total moment of inertia of the wheel and axel. I_G is the gearbox moment of inertia at the engaged gear. ω_w is the wheel angular velocity.

Based on the no slipping assumption:

$$V = \omega_w R \tag{14}$$

Using (14), the longitudinal dynamics of the vehicle yields:

$$\dot{V} = \frac{(T_w/R - Mgsin\theta - f)}{(I_b + I_w + I_G)/R^2} \tag{15}$$

In the equation above, f is the resistive force defined as:

$$f = f_{drag} + f_{roll} \tag{16}$$

I_b is the equivalent vehicle body moment of inertia defined as:

$$I_b = MR^2 \tag{17}$$

2.6 Dynamic Model Parameters

The values for the constant parameters of the dynamic model are shown in Table II.

TABLE II. DYNAMIC MODEL PARAMETERS [10]

Parameter	Value	Parameter	Value
$M(kg)$	2805	C_D	0.4
$R(m)$	0.371	$A(m^2)$	1.81×1.99
$I_w(kg.m^2)$	2.5	K_{rr}	0.015
$J_e(kg.m^2)$	0.5	$J_p(kg.m^2)$	0.1
r_{fd}	3.42	ρ (kg/m^3)	1.225
$P_{max}(hp)$	175	g (m/s^2)	9.81

The values for the gear-dependent parameters are shown in Table III for each gear. As shown in Table III, the gearbox moment of inertia is similar for all gears except for the first. Moreover, the gearbox moment of inertia is negligible compared to the wheel and equivalent moment of inertia.

TABLE III. GEAR-DEPENDENT DYNAMIC MODEL PARAMETERS [10]

Parameter	Gear 1	Gear 2	Gear 3	Gear 4
r_G	3.060	1.625	1.000	0.696

η_G	0.987	0.987	1.000	0.994
$I_G(kg.m^2)$	0.362	0.066	0.066	0.066

Consequently, a total equivalent moment of inertia (I) that is independent of the engaged gear is used in this work.

$$I \approx I_b + I_w = 388.5 \; kg.m^2 \tag{18}$$

Therefore, longitudinal dynamics can be written as:

$$\dot{V} = \frac{(T_w/R - Mgsin\theta - f)}{I/R^2} \tag{19}$$

As shown, the general state variables of dynamic model are engine RPM, gear, and velocity with their corresponding state equations as (1), (7), and (19), respectively.

$$\boldsymbol{x} = [N_e \quad G \quad V]^T \tag{20}$$

The control variables of the dynamic model are gear-shift and throttle.

$$\boldsymbol{u} = [\delta \quad G_s]^T \tag{21}$$

The primary goal of this study is to demonstrate a simplified approach to gear-shift controller design by applying it to a simple model of a typical powertrain. Therefore, gear-shift mechanisms such as clutches, gear sets, and hydraulic systems, or torque-converter lock schedule are ignored; however, same method can be modified and adapted to any of the state-of-the-art powertrains in a similar way.

3 SINGLE-STATE CONSTANT ACCELERATOR MANEUVER MODEL

In this section, the model described in the previous section is evolved in to a single-state model which applies to constant accelerator maneuvers based on wheel power interpretation of the accelerator pedal. The only state variable of this model is the gear. Because of its simplicity, all optimization problems solved in this work are based on this model.

Based on the wheel power interpretation of the accelerator, this section discusses the dynamics of the vehicle in a constant accelerator maneuver as well as the governing factors in its fuel efficiency.

A constant accelerator maneuver is the one in which the operator maintains a constant accelerator in a level road ($\theta = 0$). In this work, accelerator is interpreted as desired wheel power as:

$$P_w = \xi P_{max} \tag{22}$$

In the equation above, $0 < \xi < 1$ represents the accelerator pedal input and P_{max} is the maximum available power (Table II). The wheel power is defined as:

$$P_w = T_w V / R \tag{23}$$

Consequently the longitudinal vehicle dynamics for a constant accelerator maneuver can be written as:

$$\dot{V} = \frac{\xi P_{max}/V - 0.5\rho C_D A V^2 - K_{rr} Mg}{I/R^2} \tag{24}$$

Equation (24) is an ordinary differential equation. The steady state solution of this equation from stationary conditions is designated by $V^*(t^*)$. Therefore, for a constant accelerator maneuver velocity is no longer a state variable. The solutions for the above differential equation are depicted in Fig. 6 for 30%, 60%, and 90% accelerator. As shown in Fig. 6, with the wheel power being constant, increase in velocity

leads to an increased aerodynamic drag loss until there is no excess power available to increase the kinetic energy, and the velocity reaches steady-state velocity (V_{ss}^*).
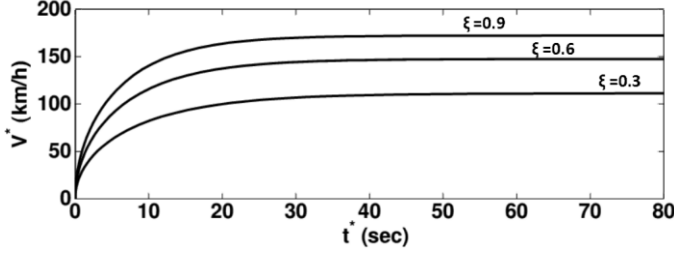

Fig. 6. Solutions of (24) for 30%, 60%, and 90% accelerator

Using (2), (3), and (10), wheel power can be written in terms of the state variables as:

$$P_w = \frac{\eta_f r_f r_T N_e^2 V}{K^2 R} \tag{25}$$

Using (4), (11), and (14), the engine RPM can be related to the velocity by the slipping ratio as:

$$N_e = \frac{60}{2\pi} \frac{r_{fd} r_G V}{r_s R} \tag{26}$$

By replacing this term for engine RPM and the analytical models of the torque converter parameters from (5) and (6), equation (25) can be written in the form of a 4th order algebraic equation as:

$$r_s^4 + l_3 r_s^3 + l_2 r_s^2 + l_1 r_s + l_0 = 0 \tag{27}$$

In above equation, the coefficients l_0 to l_3 are defined as:

$$l_0 = -c/\lambda a^2 \tag{28}$$
$$l_1 = -(d - 2c)/\lambda a^2 \tag{29}$$
$$l_2 = [(b/a) - 1]^2 - (c - 2d)/\lambda a^2 \tag{30}$$
$$l_3 = 2[(b/a) - 1] - d/\lambda a^2 \tag{31}$$

In the equations above, λ is defined as:

$$\lambda = \frac{\xi P_{max}}{\eta_{fd} \eta_G} (\frac{2\pi}{60})^2 (\frac{R}{V^* r_{fd} r_G})^3 \tag{32}$$
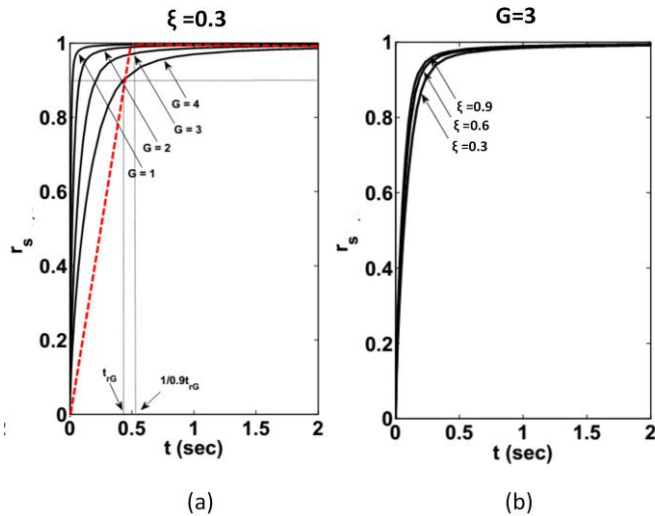

(a)   (b)

Fig. 7. (a) Solutions of (27) for 30% accelerator in G=1,2,3 and 4 (b) Solutions of (27) for 30%, 60%, and 90% accelerator in G=3

Since the solution is corresponding to a constant acceleration maneuvers from stationary conditions, it is expected that the correct solution satisfies $0 < r_s < 1$. As expected, equation (27) with values of a, b, c, and d corresponding to $r_s > 1$ leads to an inconsistent solution. Equation (27) with values of a, b, c, and d corresponding to $0 < r_s < 1$ yields four potential solutions from which only one satisfies the condition of $0 < r_s < 1$.

The solution to (27) for 30% accelerator with G=1, 2, 3, and 4 are shown in Fig. 7 (a). Fig. 7 (b) shows the solution for 30%, 60%, and 90% accelerator in the 3rd gear. Comparison of these two figures indicates that torque converter's response has low sensitivity to the accelerator and high sensitivity to the gear. Therefore, it is assumed that this response is only dependent on the gear. To express torque converter's response in a simple analytical form, it has been approximated by combination of an oblique line and a horizontal line. An example of this approximation is shown for the curve corresponding to G=4 in Fig. 7 (a). The oblique line and horizontal line are shown by dashed red lines. The oblique line intersects the original curve in 0.9 slipping ratio. The time corresponding to this intersection is referred to as rise-time and is designated by t_{r_G}. The switching from oblique line to horizontal line takes place in slipping ratio equal to 1. As a result, the time corresponding to this switching is $\frac{1}{0.9} t_{r_G}$.

In general a truck would run through the FTP75 cycle with less than 30% accelerator. As such, average of slipping ratio rise-times for 10% and 30% accelerator is chosen for the controller design purposes. This parameter is denoted by t_{r_G} for each gear, G. Table IV shows values of this parameter in each gear.

TABLE IV. SLIPPING RATIO RISE-TIME IN A CONSTANT ACCELERATOR MANEUVER

	Gear 1	Gear 2	Gear 3	Gear 4
t_{r_G} (sec)	22	103	211	**441**

Comparison of the slipping ratio rise-times in this figure with velocity rise-times in Fig. 6 indicates that the dynamics of the torque-converter is much faster than dynamics of the vehicle. The slipping ratio rise-times are less than 0.5 sec, for discrete-time analysis with sampling times longer than 0.5 sec the torque converter can be ignored in the model. Consequently, for the constant accelerator maneuver, the number of state variables reduces to one. For the single-state dynamic model the state and control vectors are defined as:

$$\hat{x} = [G]^T \tag{33}$$
$$\hat{u} = [\delta \quad G_s]^T \tag{34}$$

4   OPTIMIZATION PROBLEM

This section gives a formal statement of the optimization problem based on the single-state model.

4.1   Discretization

Table V shows span and resolutions of the discretized state and control variables.

TABLE V. STAT/CONTROL VARIABLE DISCRETIZATION

Variable	Resolution	Span
G	1	1–4
δ (%)	1	0–100
G_s	1	(-1)-(+1)

Equation (35) shows the discretized form of the state equation:

$$G_{k+1} = G_k + G_{s,k} \tag{35}$$

4.2 Constraints

In the single state model, the engine RPM limit can be interpreted in terms of velocity using (48). The acceptable velocity limit for each gear is shown in Table VI. So, the initial conditions of (24) is chosen as $V_0 = V_1^{min}$ and the initial conditions of optimization algorithm is chosen $G_0 = 1$.

TABLE VI. UPPER AND LOWER VELOCITY LIMITS OF A CONSTANT ACCELERATOR MANEUVER

	Gear 1	Gear 2	Gear 3	Gear 4
V_G^{min} (km/h)	8	15	25	36
V_G^{max} (km/h)	80	150	245	352

Since the objective of the optimization problem is to minimize the fuel consumption, the optimization algorithm, naturally, tends to decreases the wheel power. As such, definition of the constant accelerator constraint in the form of $1 < \frac{P_w}{\xi P_{max}} < 1 + \varepsilon$ will be the closest to the perfect constant accelerator maneuver assumption $(P_w = \xi P_{max})$. The appropriate choice of ε is dependent on the throttle resolution. Based on trial and error, 0.05 is selected for this parameter in the present work. A larger value is required if the throttle resolution was more coarse.

4.3 Cost Function

The objective of the proposed optimization problem is to minimize the fuel consumption. The energy balance in the powertrain is as follows:

$$E_f = E_p + E_k + E_l \tag{36}$$

In the equation above E_f is the fuel energy, E_p is the potential energy, E_k is the kinetic energy, and E_l is the energy loss. The fuel energy is calculated as

$$E_f = h_f \int \dot{m} \, dt \tag{37}$$

In the equation above, $\dot{m}$ is the fuel mass flow rate and h_f is the heat of reaction for unit mass of the fuel.

Energy loss includes the engine loss (E_{eng}), the torque converter loss (E_{tc}), and drag loss (E_{drag}).

$$E_l = E_{eng} + E_{tc} + E_{drag} \tag{38}$$

For a constant accelerator maneuver:

$$E_p = 0 \tag{39}$$

$$E_k = 0.5MV^{*2} \tag{40}$$

$$E_{drag} = 0.5\rho C_D A \int V^{*3} dt \tag{41}$$

The brake specific fuel consumption (BSFC) can be expressed as:

$$BSFC = \frac{\int \dot{m} dt}{\int V dt} \tag{42}$$

Using the energy balance equation, the specific fuel consumption for a constant accelerator maneuver can be written as:

$$BSFC = \frac{0.5\rho C_D A \int V^{*3} dt + 0.5MV^{*2} + E_{eng} + E_{tc}}{h_f \int V^* dt} \tag{43}$$

The only unknowns in (43) are E_{eng} and E_{tc}. Therefore, minimization of BSFC for a constant accelerator maneuver boils down to minimizing the combination of the torque converter loss and the engine loss. Considering the combination of the torque converter loss and the engine loss, when gear shift takes place at a higher engine RPM, torque-converter loss increases because the relative speed between the pump and turbine increases. On the other hand, engine, generally, is more efficient at relatively high RPM. So, a optimization problem is solved to optimize this tradeoff.

The cost function of the DP algorithm in N steps has the following form [27].

$$J = H(x_N) + \sum_{k=1}^{N-1} L(x_k, u_k) \tag{44}$$

In the equation above, L represents the general nonlinear dependence of the kth time-step's cost on state and control variables. H is the last time-step's cost which is only a function of the last time-step's state. The cost function of the optimization problem is defined as:

$$J = \int d\left(\frac{\dot{m}}{V}\right) \tag{45}$$

This definition is mathematically different from BSFC; however, it represents in a different way the same idea of the specific fuel consumption. This definition has three advantages: (1) it has an additive form suitable for DP algorithm. (2) It represents the idea of the specific fuel consumption in a more instantaneous sense than BSFC; so, it is more suited for a feedback control scheme. (3) Based on this definition, the loss of torque-converter can be considered in the cost function more accurately. The details of this consideration will be discussed later in this section. Discretization of this cost function to the form shown in (44) leads to:

$$L = \dot{m}_k / V_k^* \tag{46}$$

$$H = 0 \tag{47}$$

As shown in the fuel consumption characteristic diagram, fuel mass flow rate is a function of the throttle and engine RPM. Based on the single-state model ($r_s = 1$), the engine RPM is only a function of gear in a constant accelerator maneuver.

$$N_{e_{G_k}}^* = \frac{60}{2\pi} \frac{r_{fd} r_{G_k} V_k^*}{R} \tag{48}$$

Fig. 8 shows a time-step including a gear-shift from G_{k-1} to G_k. According to (26), the slipping ratios just after and just before the gear-shift are related by:

$$\frac{r_{s,k-1}^+}{r_{s,k-1}^-} = \frac{r_{G_k}}{r_{G_{k-1}}} \tag{49}$$

Based on the fast dynamics of the engine, the slipping ratio

is assumed to be unity just before the gear shift. As such:

$$r_{s,k-1}^{+} = \frac{r_{G_k}}{r_{G_{k-1}}} \tag{50}$$

The actual variation of the slipping ratio is represented by the dashed line. This variation is approximated by a line with slope as:

$$\dot{r}_s = 1/0.9 t_{r_{G_k}} \tag{51}$$

The cost function in (46) can be written as (52) by multiplying both nominator and denominator by Δt_k^*.

$$L = \dot{m}_k \Delta t_k^* / (V_k^* \Delta t_k^*) \tag{52}$$

For a time-step including a gear-shift, the nominator of the above fraction is splitted into two components. The first component represents the time period in which torque-converter's turbine and pump have non-zero relative velocity and viscous loss is present.
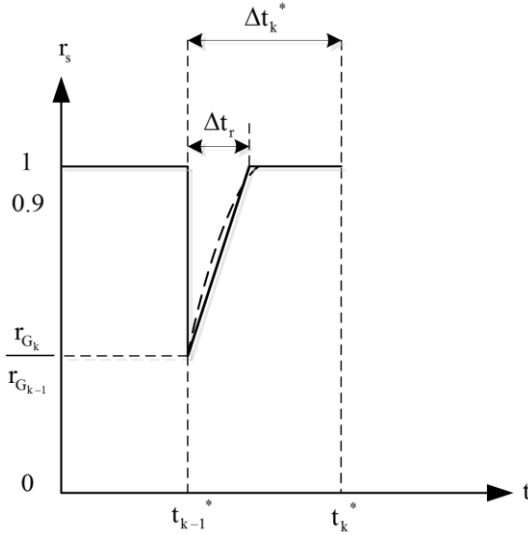
Fig. 8. Model of the torque converter behavior at a gear-shift

This time period is designated by Δt_r and can be calculated as:

$$\Delta t_r = \frac{10}{9}(1 - \frac{r_{G_k}}{r_{G_{k-1}}})t_{r_{G_k}} \tag{53}$$

The second component represents the rest of the time-step in which pump and turbine are synchronized and no viscous loss is present. To consider the torque-converter loss in the cost function calculation, the first component is written in an integral form as:

$$L_k = \frac{\int_{t_{k-1}^*}^{t_{k-1}^* + \Delta t_r} \dot{m} dt + (\Delta t_k^* - \Delta t_r)\dot{m}_k}{V_k^* \Delta t_k^*} \tag{54}$$

Through integral variable substitution from t to r_s, this term can be rearranged as:

$$\int_{t_{k-1}^*}^{t_{k-1}^* + \Delta t_r} \dot{m} dt = \int_{\frac{r_{G_k}}{r_{G_{k-1}}}}^{1} \frac{\dot{m}}{\dot{r}_s} dr_s \tag{55}$$

Replacing $\dot{r}_s$ from (51) and substituting the integral variable from (26), this integral can be calculated as:

$$\int_{\frac{r_{G_k}}{r_{G_{k-1}}}}^{1} \frac{\dot{m}}{\dot{r}_s} dr_s = V_k^* r_{G_k} t_{r_{G_k}} \left[\left[-\frac{600 r_{fd}}{18\pi R} \int_{N_{e_{G_{k-1}}}^*}^{N_{e_{G_k}}^*} \frac{\dot{m}}{N_e^2} dN_e \right]\right] \tag{56}$$

Based on the fuel consumption characteristic diagram and the vehicle dynamic model parameters, the term inside the bracket is tabulated as:

$$\Gamma(\delta, N_e) = -\frac{600 r_{fd}}{18\pi R} \int_{600}^{N_e} \frac{\dot{m}(\delta, N_e)}{N_e^2} dN_e \tag{57}$$

As shown Γ has dimension of (g/m). So, it is referred to as the gear-shift fuel consumption parameter in this work.

Fig. 9, shows the gear-shift fuel consumption parameter table. Using this parameter, the cost function for a time-step involving a gear-shift can be calculated as:

$$L_k = r_{G_k} \frac{t_{r_{G_k}}}{\Delta t_k^*}\left[\Gamma\left(\delta_k, N_{e\,G_k}^*\right) - \Gamma\left(\delta_k, N_{e\,G_{k-1}}^*\right)\right] + \frac{\dot{m}_k}{V_k^*}(1 - \frac{\Delta t_r}{\Delta t_k^*}) \tag{58}$$
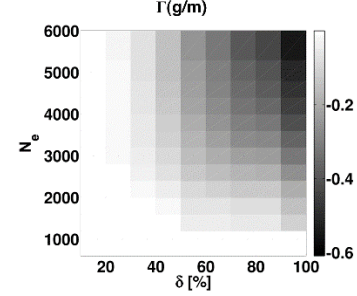

Fig. 9. Gear-shift fuel consumption parameter

Considering (53) for the definition of Δt_r, (58) can be written in the following form.

$$L_k = (1 + \alpha)\frac{\dot{m}_k}{V_k^*} \tag{59}$$

In the equation above α is gear-shift fuel consumption correction factor and is defined as:

$$\alpha = \left[\frac{\Gamma\left(\delta_k, N_{e\,G_k}^*\right) - \Gamma\left(\delta_k, N_{e\,G_{k-1}}^*\right)}{\dot{m}_k/V_k^*} r_{G_k} - \frac{10}{9}(1 - \frac{r_{G_k}}{r_{G_{k-1}}})\right]\frac{t_{r_{G_k}}}{\Delta t_k^*} \tag{60}$$

Fig. 10 presents the flowchart used to calculate k^{th} time-step's cost. As shown, the first and second steps, respectively, apply the engine RPM and constant accelerator constraints. At the third step, the algorithm uses different cost functions depending on whether or not a gear-shift is taking place.
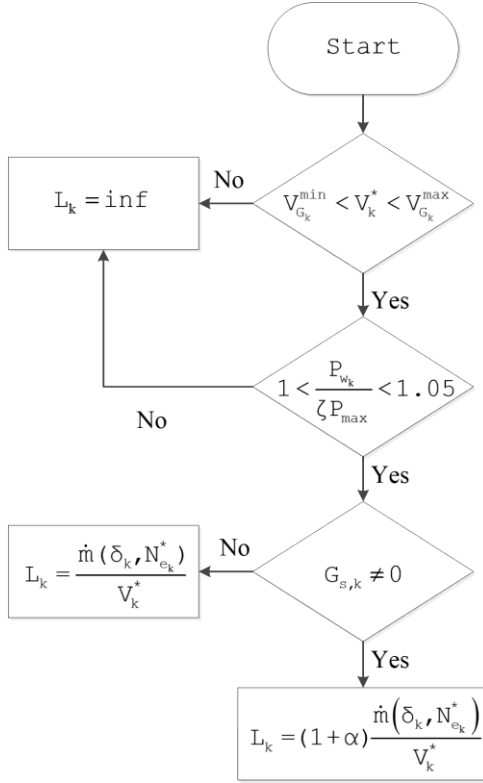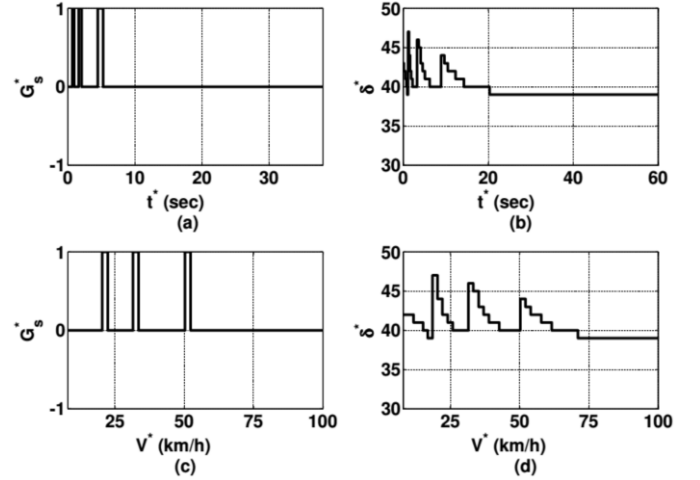
Fig. 10. Cost function calculation flowchart

Fig. 11. Solution of the optimization problem for the 30% accelerator maneuver (a) gear-shift control signal (b) throttle control signal (c) gear shift vs. velocity (d) throttle vs. velocity

4.4   Solution of the optimization problem

Fig. 11 illustrates the solution of the proposed single-state optimization problem corresponding to 30% accelerator. Fig. 11 (a) and (b) shows the optimal gear shift and throttle control signals. Fig. 11 (c) and (d) shows the optimal control variables with respect to velocity. Fig. 11 suggests that the algorithm applies throttle surge at gear-shift. Moreover, at a single gear the throttle decreases by the increase in velocity. As gear shift is applied, the engine RPM falls. Consequently, according to the engine power diagram the fuel mass flow rate decreases, and the fuel power decreases. To keep the wheel power on the reference value set by accelerator, the algorithm increases throttle to get more fuel mass flow rate. In a constant gear, increase in velocity is corresponding to increase in engine RPM. For a constant throttle, the increase in engine RPM results in more input power. Consequently, the algorithm gradually decreases throttle to keep the wheel power on the reference value set by the accelerator.

The fraction of the wheel power to the desired wheel power is shown in Fig. 12. As shown, by proposed definition of the power band, the algorithm keeps the wheel power as close to unity as possible.
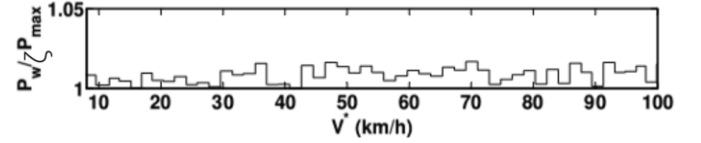

Fig. 12. Wheel power to desired wheel power ratio in the optimization problem for the 30% accelerator maneuver

5   FEEDBACK TABLE DESIGN

Fig. 13 shows the integrated gear-shift and throttle feedback tables. Gear-shift and throttle control actions are assigned as a function of the accelerator and velocity. This table is constructed by linear interpolation of the optimal control variables for 10% to 100% constant accelerator maneuvers with 10% step.

As shown, in the gear-shift look-up table, the optimal gear-shift velocities increase with accelerator because driveability requirements get stronger.

As shown, increase in accelerator, generally, leads to an increase in throttle because more mass flow rate of fuel is needed to address the wheel power demand. Furthermore, the gear-shift boundaries overlap with margins of the throttle surge discussed in the previous section. For a constant accelerator, the throttle decreases as velocity increases in each gear to keep the wheel power on the desired value.

According to (25), wheel power is a function of the general state variables (engine RPM, gear, and velocity). Therefore, the state space can also be represented by velocity, gear and wheel power (accelerator). As the proposed feedback tables assign the optimal control variables to the state space, it is expected that the proposed feedback tables be near optimal for any arbitrary maneuver and initial conditions.
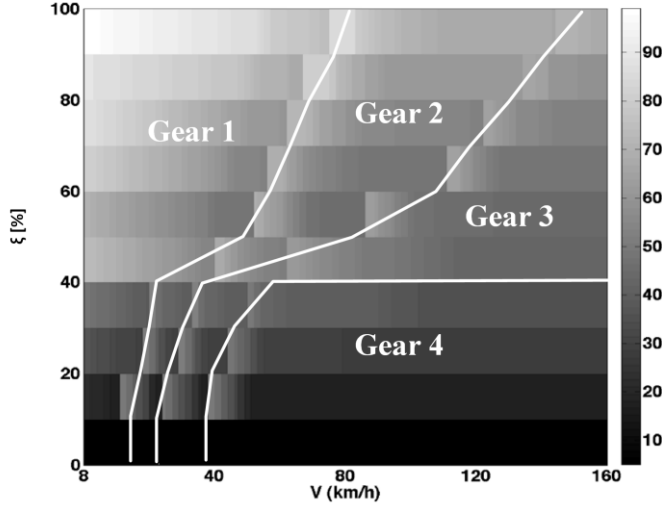
Fig. 13. Integrated Gear-shift and Throttle Feedback Tables. The color map indicates the throttle level in percent.
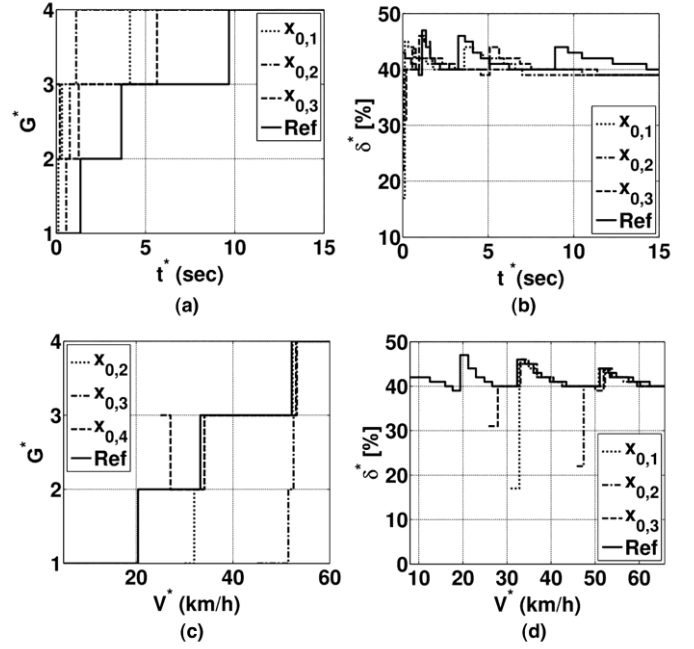

Fig. 14. Initial conditions effect on the solution of the optimization problem (a) optimal gear-shift control signal (b) optimal throttle control signal (c) optimal gear-shift vs. velocity (d) optimal throttle vs. velocity

6   SIMULATIONS

According to the previous section, it is expected that the gear-shift feedback table exhibit optimal behavior for all operating conditions of the vehicle. This section uses simulation and optimization to offer evidence of optimality for some significant cases. Moreover, a simulation is used to illustrate the impact of the throttle feedback table in enhancing the driveability.

6.1   Optimality Test

This section illustrates the optimality of the gear-shift control in non-stationary initial conditions, non-level road conditions, and non-constant accelerator maneuvers.

Non-stationary initial conditions

To evaluate the optimality of the gear-shift feedback table for different initial conditions, the optimization of the 30% accelerator maneuver is reiterated with different initial conditions. Table VII shows the initial conditions setup of the optimization problems. Fig. 14 (a) and (b) shows comparison of the optimal control signals for each case compared to the reference optimization problem solved in section 4. As shown the control signals are completely different when plotted against time; however, Fig. 14 (c) and (d) shows that they overlap when plotted against velocity. This indicates that the designed feedback tables would perform optimal control when it is used for any of these three cases.

TABLE VII - INITIAL CONDITIONS FOR OPTIMIZATION PROBLEMS 1 TO 3

Problem	$V_0(km/h)$	G_0
1	30	1
2	45	1
3	25	3

Non-level road conditions

According to the definition of the constant accelerator maneuver, optimization problems are solved for level road conditions. In practice, the vehicle would experience considerable road slope. Therefore, optimal performance would not be achieved if the optimized gear-shift control was applied with an open-loop approach. To evaluate the optimality of the gear-shift feedback table for non-level road, the optimization of the 30% accelerator maneuver is reiterated for a 10° up-hill condition.

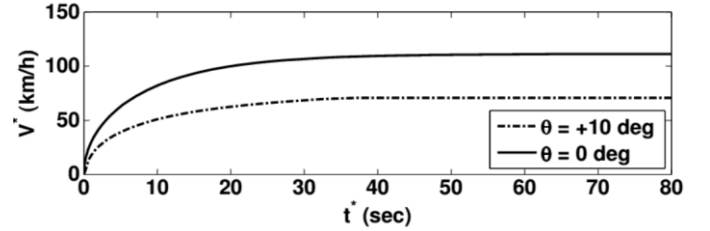Fig. 15 shows the effect of +10° road gradient on the velocity.

Fig. 15. Effect of +10 degrees road gradient on the velocity of the 30% accelerator maneuver

As a portion of the wheel power is stored as potential energy, velocity reaches the steady-state conditions in a lower value; however, optimal control variables overlap when plotted against velocity (Fig. 16 (a) and Fig. 16 (b)). This indicates that the designed feedback tables would perform optimal control when it is used in an up-hill condition.
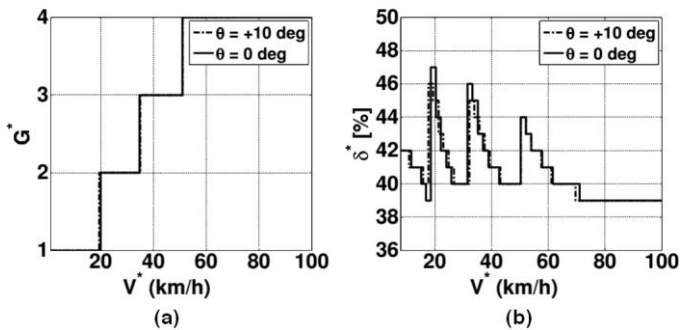
Fig. 16. Effect of +10 degrees road gradient on optimization of the 30% accelerator maneuver (a) optimal gear-shift vs. velocity (b) optimal throttle vs. velocity

Non-constant maneuvers

Constant accelerator maneuvers are the main maneuvers in long distance trips playing a crucial role in the fuel economy of the vehicle; however, non-constant accelerator maneuvers in short-distance travels within urban area have a stronger environmental impact. Therefore optimality of the gear-shift control has significance in non-constant accelerator maneuvers. In this section, a simulation demonstrates the optimality of the gear-shift control in a ramp accelerator maneuver as $\xi = 0.9 - 0.04t$. The proposed gear-shift control is contrasted by the optimal gear-shift strategy obtained by optimizing the maneuver.
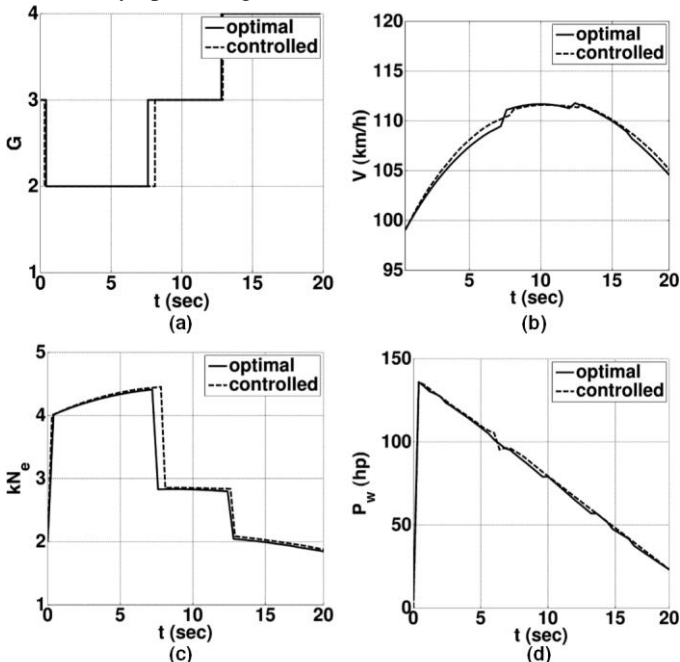

Fig. 17. Comparison of the state variable trajectories in the controlled strategy with the optimal strategy (truth) ; (a) gear trajectory; (b) velocity trajectory; (c) engine RPM trajectory; (d) wheel power

The optimization is performed by the single-state DP algorithm developed in section 4. In simulation, the detailed dynamic model developed in section 2 is used as the plant.

Fig. 17 (a), (b), and (c) shows state variable trajectories in controlled strategy compared to the optimized strategy.
Fig. 17 (d) shows the wheel power during the maneuver. As shown, feedback tables not only track the reference power, but

also the gear-shift control is in consistent with the optimal solution. A state space visualization of this maneuver is presented in Fig. 18. According to the presented view, the feedback table controls the state variable trajectories on the optimal trajectory. Moreover, the boundaries within the gear-shift feedback table are corresponding to optimal gear-shift states for arbitrary maneuvers.

As mentioned in section 5, in each optimization problem, the optimal control variables beyond the steady state curve are assigned equal to the optimal control variable in the last time-step. As shown in Fig. 18 a portion of the simulated maneuver crosses over the steady state curve. However, the simulation results indicate that power tracking is not degraded in this portion.
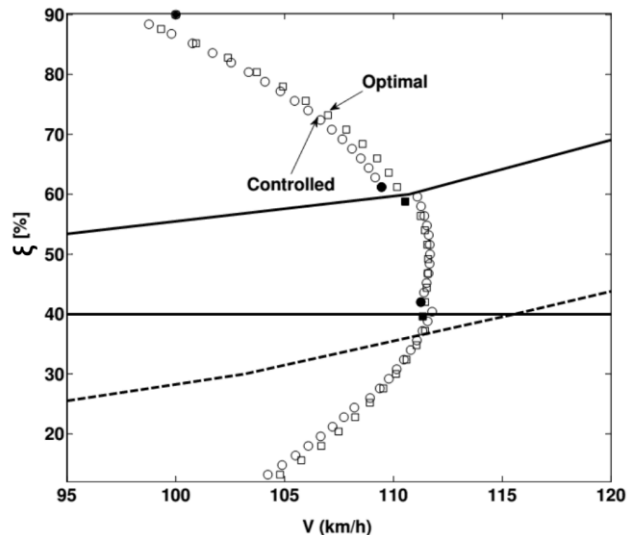

Fig. 18. Comparison of the state space path of the controlled strategy and the optimal strategy (truth) in the ramp accelerator maneuver

6.2 Quasi-static Simulation

This section uses quasi-static method [19] to simulate the fuel economy of the proposed controller in some benchmark driving cycles. Simulations are performed using QSS Toolbox [28] developed by IMRT (Measurements and Control Laboratory) in ETH Zurich (Swiss Federal Institute of Technology Zurich). The standard gear-shift patterns in this package are used as the reference.
Fig. 19 shows the general simulation setup. The solid line shows the standard configuration of the quasi-static model of the vehicle [19]. The proposed controller is incorporated in the model as shown by the dashed lines. For each cycle, the proposed controller is considered in two forms. In the first form, the proposed gear-shift feedback table is used directly. In the second form, an 8 km/h gear-shift hysteresis margin is added to the proposed gear-shift feedback table.
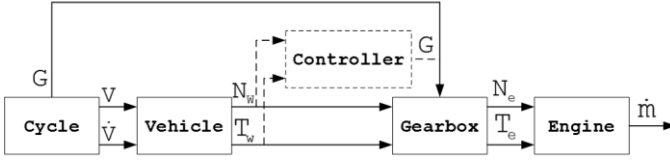
Fig. 19. Quasi-static Simulation Setup; the dashed parts show alternative configuration based on the proposed gear-shift feedback table

A truck generally runs through the FTP75 cycle. Fig. 20 shows the simulation results for this cycle. Fig. 20 (a) shows the gear-shift patterns of the three cases studied in this simulation. The standard gear-shift pattern is designated by the solid line. The dashed-dot and dashed lines are the gear-shift patterns of the proposed controller with and without hysteresis, respectively. As shown, the proposed controller (with or without hysteresis), tends to operate the vehicle at higher gears compared to the standard gear-shift pattern. This strategy stems from the proposed optimization. This gear-shift pattern keeps the engine at a relatively lower RPM which leads to less loss in engine and torque-converter during gear-shifts while satisfying desired wheel power demand. Fig. 20 (b) shows the difference between the fuel consumption rate of in the controlled gear-shift patterns and the standard gear-shift pattern. While optimization problems were not solved for this driving cycle, the fuel consumption rate of the proposed controller without hysteresis is less than the standard gear-shift strategy in all moments of the driving cycle (rather than in a cumulative sense). This indicates optimality of the designed controller in a feedback sense that makes it favorable for real-time implementation.

Table VIII shows the quantitative results of the simulation. As shown, the proposed controller, without hysteresis, reduces the cumulative specific fuel consumption by 9.9% for FTP75 cycle. This improvement is unrealistic because it sacrifices driveability. While this controller guarantees driver's power demand satisfaction, there are two major issues with driveability of this controller. First of all, according to Fig. 20, operating gear in this controller is almost always higher than other strategies. This leads to a lower power reserve margin. Power reserve margin represents acceleration capability and is defined as the difference between the current power and maximum achievable power in each instant. Table VIII shows the accumulated power reserve (APR) for different gear-shift strategies. As shown, the 9.9% fuel economy improvement of the controller without hysteresis is achieved at the cost of significant APR penalty. The second driveability issue of the controller without hysteresis is the multiple tandem gear-shifts in a short time interval which are clearly demonstrated in Fig. 1 (a). Industry sacrifices some fuel economy to avoid driveability issues. To take this into consideration, an 8 km/h gear-shift hysteresis margin is added to the boundaries of the optimal gear-shift feedback table. As shown in Fig. 20 (a) the hysteresis has eliminated the tandem gear-shift problem. Moreover, APR is significantly improved over the controller without hysterisis. While, fuel economy is compromised with application of the hysteresis, the gear-shift strategy still benefits from the optimization because as shown in Fig. 20 (b) the fuel consumption rate diagram of the controller with hysteresis generally follows the one for the controller without hysteresis.
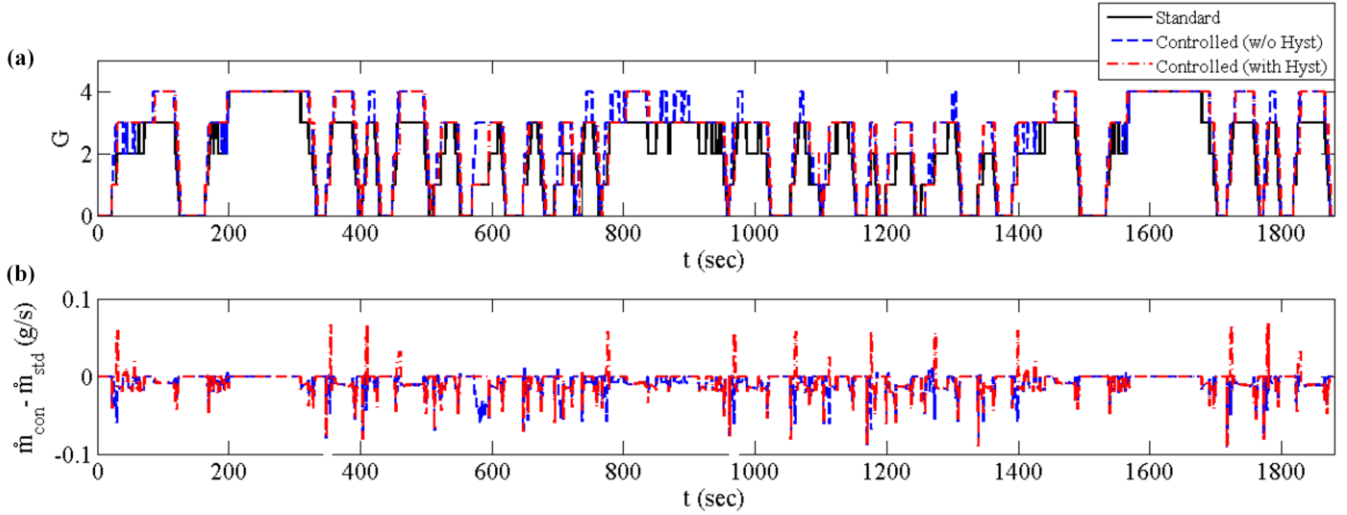

Fig. 20. Comparison of the Standard Gear-shift Strategy and Controlled Gear-shift Strategy for EPA Cycle (a) Gear-shift Pattern (b) Fuel Consumption Rate

The reason of increase in fuel consumption is untimely gear-shifts leading to jumps in fuel consumption rate for a short time periods as shown in Fig. 20 (b). According to the quantitative results shown in Table VIII, after application of the hysteresis, the fuel economy advantage is still significant while the APR is not compromised considerably. This indicates that the controller with hysteresis can improve fuel

economy while offering an acceptable level of driveability.

Comparing driving aggressive, high speed driving cycles, e.g. FTP—highways, with mild driving cycles, e.g. FTP75 and NEDC, it is observed that, BSFC is considerably less for FTP—highways because of low engine RPM operation and less gear-shifts. Furthermore, the high wheel power demand required to follow the aggressive driving cycles is more likely

to satisfy the driveability level by default, thus benefitting less from the optimization of fuel economy.

This controller is designed in a feedback for which indicates real-time implementability despite many optimization-based methods in the literature. Compared to production maps, while the designed controller has slightly less APR, it considerable benefits from fuel economy. Moreover, its optimality is guaranteed, theoretically, for constant accelerator maneuver.

Constant accelerator maneuver is a dominant maneuver in long distance trips and play a significant role in the overall fuel efficiency of the vehicle. From a practical point of view, it only takes a couple of days to construct gear/throttle map by this approach, whereas the practice of constructing the conventional production maps takes several months and are refined by highly experienced calibration engineers for many years.

TABLE VIII – SIMULATION RESULTS FOR THE BSFC AND APR

Driving cycle	APR (kJ/100km) $\times 10^5$			BSFC (lit/100km)		
	Standard	Controlled w/o Hyst	Controlled with Hyst	Standard	Controlled w/o Hyst	Controlled with Hyst
FTP75	1.09	0.99 (-9.5%)	1.07 (-2.1%)	12.1	10.9 (-9.9%)	11.2 (-7.4%)
NEDC	1.11	0.98 (-11.7%)	1.07 (-3.3%)	11.8	10.7 (-9.3%)	11.0 (-6.8%)
FTP—highways	0.57	0.55 (-3.1%)	0.56 (-1.2%)	9.6	9.4 (-2.1%)	9.5 (-1.0%)

7 CONCLUSION

An integrated control of gear-shift and throttle is developed based on the DP algorithm. Accelerator is interpreted as the desired wheel power, and the objective is to achieve the desired wheel power with maximum fuel efficiency. The DP optimization problem is solved for constant accelerator maneuvers based on a single-state model. A technique is proposed to include the torque-converter loss in the single-state optimization problem. Solutions of the optimization problems are used to design feedback tables for real-time control.

Based on simulations, the gear-shift control is consistent with the optimal strategy independent of the initial conditions, road slopes, and accelerator maneuvers. Based on quasi-static simulations, the controller provides significant advantage in fuel economy while providing an acceptable level of driveability.

REFERENCES

[1] T. W. Birch, C. Rockwood, and T. Birch, *Automatic transmissions and transaxles*: Pearson Prentice Hall, 2006.

[2] W. Wang, *Dynamic powertrain system modeling and simulation with applications for diagnostics, design and control*: University of Wisconsin--Madison, 2000.

[3] A. F. A. Serrarens, "Coordinated control of the zero inertia powertrain," 2001.

[4] S. Takahashi, "Fundamental study of low fuel consumption control scheme based on combination of direct fuel injection engine and continuously variable transmission," in *Decision and Control, 1998. Proceedings of the 37th IEEE Conference on*, 1998, pp. 1522-1529.

[5] M. Yasuoka, M. Uchida, S. Katakura, and T. Yoshino, "An integrated control algorithm for an Sl engine and a CVT," *SAE. Trans.,* vol. 108, pp. 1369-1374, 1999.

[6] J. Fredriksson and B. Egardt, "Nonlinear control applied to gearshifting in automated manual transmissions," in *Proc. IEEE. Conf. Decision. Cont*, 2000, pp. 444-449 vol.1.

[7] T. Minowa, H. Kimura, N. Ozaki, and M. Ibamoto, "Improvement of fuel consumption for a vehicle with an automatic transmission using driven power control with a powertrain model," *JSAE Rev,* vol. 17, pp. 375-380, 1996.

[8] H. Vahabzadeh and S. M. Linzell, "Modeling, Simulation, and Control Implementation for a Split-Torque, Geared Neutral, Infinitely Variable Transmission, SAE Int, 910409," 1991.

[9] V. D. Ngo, J. A. C. Navarrete, T. Hofman, M. Steinbuch, and A. Serrarens, "Optimal gear shift strategies for fuel economy and driveability," *Proceedings of the Institution of Mechanical Engineers, Part D: Journal of Automobile Engineering,* p. 0954407013491240, 2013.

[10] D. Kim, H. Peng, S. Bai, and J. M. Maguire, "Control of Integrated Powertrain With Electronic Throttle and Automatic Transmission," *Control Systems Technology, IEEE Transactions on,* vol. 15, pp. 474-482, 2007.

[11] M. H. Smith, E. J. Barth, N. Sadegh, and G. J. Vachtsevanos, "The horsepower reserve formulation of driveability for a vehicle fitted with a continuously variable transmission," *Vehicle System Dynamics,* vol. 41, pp. 157-180, 2004.

[12] A. G. Ulsoy, H. Peng, and M. Çakmakci, *Automotive control systems*: Cambridge University Press, 2012.

[13] S. Sakaguchi, E. Kimura, and K. Yamamoto, "Development of an Engine-CVT Integrated Control System, SAE Int, 1999-01-0754," 1999.

[14] R. Bellman, *Dynamic Programming*: Dover Publications, 2013.

[15] D. E. Kirk, *Optimal control theory: an introduction*: Courier Dover Publications, 2012.

[16] B. Gluss, *An Elementary Introduction to Dynamic Programming: A State Equation Approach*: Allyn and Bacon, 1972.

[17] I. McCausland, *Introduction to Optimal Control*: R.E. Krieger Publishing Company, 1977.

[18] D. Ngo, T. Hofman, M. Steinbuch, A. Serrarens, and L. Merkx, "Improvement of fuel economy in Power-

Shift Automated Manual Transmission through shift strategy optimization-an experimental study," in *Vehicle Power and Propulsion Conference (VPPC), 2010 IEEE*, 2010, pp. 1-5.

[19] L. Guzzella and A. Sciarretta, *Vehicle propulsion systems*: Springer, 2007.

[20] A. Sciarretta and L. Guzzella, "Control of hybrid electric vehicles," *Control Systems, IEEE,* vol. 27, pp. 60-70, 2007.

[21] S. Bai, J. Maguire, and H. Peng, *Dynamic Analysis and Control System Design of Automatic Transmissions*: Society of Automotive Engineers, 2013.

[22] A. Haj-Fraj and F. Pfeiffer, "Optimal control of gear shift operations in automatic transmissions," *Journal of the Franklin Institute,* vol. 338, pp. 371-390, 2001.

[23] Q. Guihe, G. Anlin, Z. Jiehong, and L. Ju-Jang, "Cruise control of automated manual transmission vehicles," *Computing & Control Engineering Journal,* vol. 14, pp. 18-21, 2003.

[24] A. Casavola, G. Prodi, and G. Rocca, "Efficient gear shifting strategies for green driving policies," in *American Control Conference (ACC), 2010*, 2010, pp. 4331-4336.

[25] B. Mashadi, A. Kazemkhani, and R. B. Lakeh, "An automatic gear-shifting strategy for manual transmissions," *Proc. Instit. Mech. Eng, Part I: J. Sys. Cont. Eng,* vol. 221, p. 757, 2007.

[26] Z. Yang, C. Cao, and Y. Su, "A method of optimal shift control based on pattern recognition and learning algorithm," in *Intelligent Control and Automation, 2002. Proceedings of the 4th World Congress on*, 2002, pp. 955-959.

[27] D. E. Kirk, "Dynamic Programming" in Optimal Control Theory: An Introduction, Mineola, New York, Dover Publications, Inc. 1998,

[28] http://www.idsc.ethz.ch/Downloads/qss/